Hindawi
Wireless Communications and Mobile Computing
Volume 2021, Article ID 5550825, 7 pages
https://doi.org/10.1155/2021/5550825

Research Article

Tradeoff-HARQ Scheme for Full-Duplex SWIPT DF Relay

Xiaoye Shi, Haiting Zhu, Fei Ding, Zhaowei Zhang, and Nan Bao

School of Internet of Things, Nanjing University of Posts and Telecommunications, Nanjing 210003, China

Correspondence should be addressed to Xiaoye Shi; shixy187@njupt.edu.cn

Received 28 January 2021; Accepted 15 October 2021; Published 25 October 2021

Academic Editor: Miaowen Wen

The SWIPT (simultaneous wireless information and power transfer) DF (decoding and forwarding) relay system could achieve the purpose of both increasing revenue and reducing expenditure. By analysing the system model and transmission characteristics of full-duplex relay, this paper optimizes the retransmission slot structure to enhance the system performance. Firstly, the state transition model is established based on the analysis of the retransmission slot structure. Secondly, the state probability of each state and the transition probability between states are calculated to obtain the total data passing rate, energy transmission efficiency, and total transmission time. Thirdly, in order to compare the performance of various HARQ (hybrid automatic repeat request) schemes more effectively, JNTP (joint normalized throughput of information transmission and energy transmission) is constructed. Monte Carlo simulations finally confirm that the proposed tradeoff-HARQ scheme outperforms the regular-HARQ scheme in terms of JNTP: the performance of the tradeoff-HARQ scheme is 0.03883 higher than that of the regular-HARQ scheme when the total power limit is 20 dB and 0.00651 higher than that of the regular-HARQ scheme when the total power limit is 30 dB.

1. Introduction

The SWIPT (simultaneous wireless information and power transfer) relay system could promote both increasing revenue and reducing expenditure of energy [1]. It is an important technology of green communication [2–4]. Xiaomi Corporation recently officially released its self-developed space isolation SWIPT technology, realizing the practical application of indoor SWIPT technology. The SWIPT relay system is regarded as the ultimate solution for mobile devices by collecting the energy in radiofrequency signals to charge the equipment and prolong the service life of the equipment [5–7]. Meanwhile, the relay can be easily deployed in the near range of equipment, which can improve the efficiency of information transmission and energy transmission at the same time [8]. In reference [9], the two-hop cooperative transmission of SWIPT relay was studied. Multiple antennas at the relay are divided into two disjoint groups for information decoding and energy acquisition, respectively. Reference [10] studied the feasibility of using relay-assisted large-capacity MIMO (multiple input multiple output) to improve the performance of wireless SWIPT. The key idea is to use the redundant degrees of freedom provided by a large number of base station antenna arrays to transmit power and information to the direct/relay users at the same time.

In order to ensure the reliable transmission of high-speed data, the system includes effective error detection and retransmission technology. The HARQ (hybrid automatic repeat request) strategy consists of two parts: (1) error detection, the receiving port will receive the data error detection, if the data is wrong, start retransmission and (2) retransmission, using the reverse link to request the source side to send again [11, 12]. In reference [13], the influence of low-power transmission strategy and incomplete channel state information on outage probability of HARQ-assisted nonorthogonal multiple access systems was obtained by using integral domain partition method and extended to the scenarios with any number of users. Reference [14] revealed the retransmission scheme of hybrid automatic repeat request for uplink transmission in large-scale cellular networks and deeply understands the influence of network parameters (such as power control parameters) on the uplink coverage performance. A new HARQ scheme for the internet of things relay was proposed: if the

acknowledgement signal is negative, the relay will select an appropriate high-order modulation constellation to transmit the source signal in one transmission slot or several time slots; if there is no error, the source will continue to transmit [15]. In reference [16], a generalized two-dimensional discrete time Markov chain model was established, and the state transition probability is analysed. By calculating the steady-state distribution of Markov chain, the closed expressions of throughput and energy efficiency of future vehicular mobile networks are derived.

Although the research on HARQ technology of SWIPT system has broad research potential, the current research is not sufficient. In reference [17], HARQ was introduced into the SWIPT direct link, and an optimal strategy aiming at the minimum expected retransmission times is proposed. The strategy only uses the received RF signal to obtain energy or accumulate mutual information. Based on the deliberate thoughts on the slot structure of the full-duplex SWIPT DF (decoding and forwarding) relay, this paper proposes a tradeoff-HARQ scheme and analyses its performance considering information transmission and energy acquisition at the same time. The main contributions in this paper are summarized as follows: (a) This paper analyses the retransmission slot structure according to the system model of the full-duplex SWIPT DF relay. (b) The state transition model is established, the transition probability between states is calculated, and then, the state transition matrix is constructed. (c) According to the initial state and state transition matrix, the state probability is calculated to obtain the total data passing rate, energy collection efficiency, and transmission time. (d) In order to compare the performance of various HARQ schemes more effectively, joint normalized throughput of information transmission and energy transmission is constructed after the parameters are normalized.

2. System Model of the Full-Duplex SWIPT DF Relay

As shown in Figure 1, the full-duplex DF relay system consists of base station B, relay R, and destination user D. Both the base station and the user are in a single-antenna half-duplex mode. The relay is equipped with two antennas in full-duplex mode; that is, it can receive the signal sent by the base station and relay the signal to the destination user at the same time. The channel fading of BR and RD is represented by h_{SR} and h_{RD}, respectively, which is a complex Gaussian distribution with a mean value of zero and variance of σ_{SR}^2 and σ_{RD}^2, respectively. The equivalent noise $n_i(i \in \{R, D\})$ at the receiver i is a complex Gaussian distribution with a mean value of 0 and a variance of N_0. Some negative factors, such as the error of the nonlinearity of the amplifier and self-interference estimation and reconstruction, may lead to the self-interference SI_R caused by full duplex. Due to the recent development of self-interference cancellation technology, the full-duplex transceiver can simultaneously transmit and receive signals in the same frequency band, and the performance gap caused by self-interference is far less than other interference signals [18, 19]. h_{ii} represent the channel fading of the self-interference channel, which is the Gaussian distribution of mean zero and variance σ_{RR}^2.

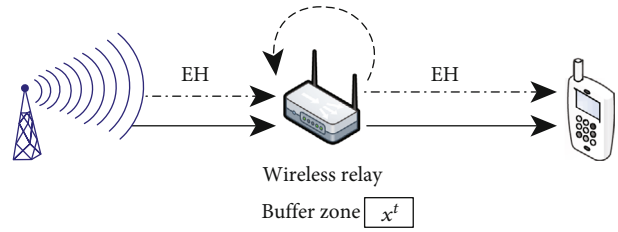

Figure 1: The system model graph of the full-duplex SWIPT DF relay.

A buffer is set at relay R to store the received data x^t temporarily. Without losing generality, it is assumed that the feedback signal can be received without error and delay and the number of retransmissions of HARQ is limited (it is assumed that the number is $M - 1$). The transmission signal of S is the complex Gaussian distribution with a mean value of 0 and variance of 1, and the error correcting code can reach the channel capacity. The receiver of each link performs CRC (cyclic redundancy check) verification, and the verification result is fed back to the transmitter through the feedback link:

(a) The identifier θ_1^t reflects whether the relay has successfully received the feedback signal of the tth frame data, $\theta_1^t = 0$ indicates the state that the relay has successfully received the tth frame data, and $\theta_1^t = 1$ indicates the unsuccessful state

(b) The identifier θ_2^t reflects whether the t-1 frame data in the R-D link is successfully received, $\theta_2^t = 0$ indicates the state that the relay has successfully received the previous frame data, and $\theta_2^t = 1$ indicates the unsuccessful state

3. Slot Structure and State Transition Model

To take into account both information transmission and energy acquisition, each transmission frame (assuming that the frame length is FL, and the time required to transmit a frame is FT, which remains unchanged in the system) is divided into two time slots: information transmission slot and energy transmission slot. The occupied time of information transmission slot is αFT, and the energy transmission slot is $(1\text{-}\alpha)$FT ($0 \le \alpha \le 1$ is the proportion of information transmission slot).

According to the state of the two links, the system is divided into four states (τ is used to mark the actual number of transmitted data frames; $\tau \le t$ is used to mark the actual number of transmitted data frames):

(a) Double normal data frames, denoted as $G_{0,0}$, i.e., $\theta_1^t = 0$ and $\theta_2^t = 0$. Both links BR and RD continues to

transmit new data frames. The expression of the received signals of link *RD* and link *BR* is as follows:

$$\begin{aligned} y_{RD}^{t} &= h_{RD}^{t}\sqrt{E_R}x^{\tau\text{-}1} + n_{RD}^{t}, \\ y_{BR}^{t} &= h_{BR}^{t}\sqrt{E_B}x^{\tau} + h_{RR}^{t}\sqrt{E_R}x^{r-1} + n_{BR}^{t} \end{aligned} \tag{1}$$

(b) Double retransmit frame, denoted as $G_{1,1}$, i.e. $\theta_1^t = 1$ and $\theta_2^t = 1$. Links *BR* and *RD* goes on retransmit the data of the previous frame. The expression of the received signals of link *RD* and link *BR* is as follows:

$$\begin{aligned} y_{RD}^{t} &= h_{RD}^{t}\sqrt{E_R}x^{\tau\text{-}1} + n_{RD}^{t}, \\ y_{BR}^{t} &= h_{BR}^{t}\sqrt{E_B}x^{\tau} + h_{RR}^{t}\sqrt{E_R}x^{\tau\text{-}1} + n_{BR}^{t} \end{aligned} \tag{2}$$

(c) Relay energy collection-relay retransmits frame, denoted as $G_{0,1}$, i.e., $\theta_1^t = 0$ and $\theta_2^t = 1$. In this case, the receiving antenna of the relay is used to collect energy, and the transmitting antenna is used to retransmit the data of the previous frame. The expression of the received signal of the link *RD* is as follows:

$$y_{RD}^{t} = h_{RD}^{t}\sqrt{E_R}x^{\tau\text{-}1} + n_{RD}^{t} \tag{3}$$

(d) Destination user energy collection-base station retransmits frame, which is recorded as $G_{1,0}$, that is, $\theta_1^t = 1$ and $\theta_2^t = 0$. In this case, the user's receiving antenna is used to collect energy, and the base station retransmits the data of the previous frame. The expression of the received signal of link *BR* is as follows:

$$y_{BR}^{t} = h_{BR}^{t}\sqrt{E_B}x^{\tau} + h_{RR}^{t}\sqrt{E_R}x^{\tau\text{-}1} + n_{BR}^{t} \tag{4}$$

Without losing generality, it is assumed that all channels obey quasistatic Rayleigh fading, that is, the transmission quality of the channel does not change in the retransmission frame. According to the received signal expression of each frame, the average SNR of links *BR* and *RD* are illustrated in equations (5) and (6), respectively.

$$\bar{\mu}_{BR} = \frac{E\left[E_B|h_{BR}|^2\right]}{\left(E\left[E_R|h_{RR}|^2\right] + N_0\right)} = \frac{E_B\sigma_{BR}^2}{E_R\sigma_{RR}^2 + N_0}, \tag{5}$$

$$\bar{\mu}_{RD} = \frac{E\left[E_R|h_{RD}|^2\right]}{N_0} = \frac{E_R\sigma_{RD}^2}{N_0}. \tag{6}$$

The data rate threshold required by the system is recorded as T. According to the definition of channel capacity and outage probability, the outage probability $P_{RD}(R)$ on link *RD* is $1 - \exp\left(-(2^T - 1)/\bar{\mu}_{RD}\right)$. Therefore, after transmitting the same data m times in the *RD* channel and combining the received signals with the maximum ratio, the outage probability $P_{RD}^{(m)}(T)$ is approximately equal to $(2^T - 1)^m/m! * (\bar{\mu}_{RD})^m$.

Figure 2 shows the system state transition diagram. According to whether *R* and *D* receive the data packet successfully or not, it can be divided into five types of states:

(a) $F_{0,0}$ indicates the normal transmission state and links *BR* and *RD* transmit new data

(b) $F_{m,0}$ represents the relay retransmission state; that is, after the relay transmits m times, the relay successfully receives the τ frame data, but *D* still does not receive the τ-1 frame data successfully

(c) $F_{0,m}$ indicates the retransmission status of the base station; that is, *D* successfully receives the τ-1 frame data after m times of transmission, but the relay still fails to receive the τ frame data

(d) $F_{m,m}$ indicates the retransmission status of the base station and relay; that is, the *R* transmits m times, and *B* transmits m times, but *D* fails to receive the τ-1 frame data and *R* fails to receive the τ frame data

(e) $S_{m,m}$ indicates *R* and *D* successfully receive the data after m times of transmission

The state transition probability is calculated according to the independent event formula and conditional probability formula:

$$\begin{aligned} P(F_{m\text{-}1,m\text{-}1} \longrightarrow F_{m,m}) &= \frac{P_{BR}^{(m)}(T)}{P_{BR}^{(m\text{-}1)}(T)}\frac{P_{RD}^{(m)}(T)}{P_{RD}^{(m\text{-}1)}(T)}, \\ P(F_{m\text{-}1,m\text{-}1} \longrightarrow F_{m,0}) &= \frac{P_{BR}^{(m)}(T)}{P_{BR}^{(m\text{-}1)}(T)}\frac{\left(1\text{-}P_{RD}^{(m)}(T)\right)}{P_{RD}^{(m\text{-}1)}(T)}, \\ P(F_{m\text{-}1,m\text{-}1} \longrightarrow F_{0,m}) &= \frac{\left(1\text{-}P_{BR}^{(m)}(T)\right)}{P_{BR}^{(m\text{-}1)}(T)}\frac{P_{RD}^{(m)}(T)}{P_{RD}^{(m\text{-}1)}(T)}, \\ P(F_{m\text{-}1,m\text{-}1} \longrightarrow S_{m,m}) &= \frac{\left(1\text{-}P_{BR}^{(m)}(T)\right)}{P_{BR}^{(m\text{-}1)}(T)}\frac{\left(1\text{-}P_{RD}^{(m)}(T)\right)}{P_{RD}^{(m\text{-}1)}(T)}. \end{aligned} \tag{7}$$

Therefore, the state transfer equation is as follows:

$$\begin{bmatrix} P(S_{m,m}) \\ P(F_{m,0}) \\ P(F_{0,m}) \\ P(F_{m,m}) \end{bmatrix} = H_{m\text{-}1} * \begin{bmatrix} P(S_{m\text{-}1,m\text{-}1}) \\ P(F_{m\text{-}1,0}) \\ P(F_{0,m\text{-}1}) \\ P(F_{m\text{-}1,m\text{-}1}) \end{bmatrix}, \tag{8}$$

where the state transition matrix is

$$H_{m\text{-}1} = \begin{bmatrix} 0 & \left(1\text{-}\frac{P_{BR}^{(m)}(T)}{P_{BR}^{(m\text{-}1)}(T)}\right) & \left(1\text{-}\frac{P_{RD}^{(m)}(T)}{P_{RD}^{(m\text{-}1)}(T)}\right) & \left(1\text{-}\frac{P_{BR}^{(m)}(T)}{P_{BR}^{(m\text{-}1)}(T)}\right) * \left(1\text{-}\frac{P_{RD}^{(m)}(T)}{P_{RD}^{(m\text{-}1)}(T)}\right) \\ 0 & \frac{P_{BR}^{(m)}(T)}{P_{BR}^{(m\text{-}1)}(T)} & 0 & \frac{P_{BR}^{(m)}(T)}{P_{BR}^{(m\text{-}1)}(T)} * \left(1\text{-}\frac{P_{RD}^{(m)}(T)}{P_{RD}^{(m\text{-}1)}(T)}\right) \\ 0 & 0 & \frac{P_{RD}^{(m)}(T)}{P_{RD}^{(m\text{-}1)}(T)} & \left(1\text{-}\frac{P_{BR}^{(m)}(T)}{P_{BR}^{(m\text{-}1)}(T)}\right) * \frac{P_{RD}^{(m)}(T)}{P_{RD}^{(m\text{-}1)}(T)} \\ 0 & 0 & 0 & \frac{P_{BR}^{(m)}(T)}{P_{BR}^{(m\text{-}1)}(T)} * \frac{P_{RD}^{(m)}(T)}{P_{RD}^{(m\text{-}1)}(T)} \end{bmatrix}. \tag{9}$$

$F_{0,0}$ is the initial state, and its state probability is $P(F_{0,0}) = 1$.

The probability of each state is calculated by the state transition equation:

$$\begin{aligned} P(F_{m,m}) &= P_{BR}^{(m)}(T)P_{RD}^{(m)}(T), \\ P(F_{m,0}) &= P_{BR}^{(m)}(T)\left(1\text{-}P_{RD}^{(m)}(T)\right), \\ P(F_{0,m}) &= \left(1\text{-}P_{BR}^{(m)}(T)\right)P_{RD}^{(m)}(T), \end{aligned}$$

$$\begin{aligned} P(S_{m,m}) = {} & \left(P_{BR}^{(m\text{-}1)}(T)\text{-}P_{BR}^{(m)}(T)\right)\left(1\text{-}P_{RD}^{(m\text{-}1)}(T)\right) \\ & + \left(P_{RD}^{(m\text{-}1)}(T)\text{-}P_{RD}^{(m)}(T)\right)\left(1\text{-}P_{BR}^{(m\text{-}1)}(T)\right) \\ & + \left(P_{BR}^{(m\text{-}1)}(T)\text{-}P_{BR}^{(m)}(T)\right)\left(P_{RD}^{(m\text{-}1)}(T)\text{-}P_{RD}^{(m)}(T)\right). \end{aligned} \tag{10}$$

4. Joint Normalized Throughput of Information Transmission and Energy Transmission

No matter whether the link BR or RD fails to decode the data after reaching the limit of transmission times, the transmission data will be discarded. Thus, after M-1 retransmissions (i.e., M transmissions), the states that the system still fails including $F_{M,0}$, $F_{0,M}$, and $F_{M,M}$. The outage probability is the sum of the above state probabilities. Substituting the probabilities of each state, the outage probability of the system is obtained as follows:

$$\begin{aligned} P_{\text{out}} &= P(F_{M,0}) + P(F_{0,M}) + P(F_{M,M}) \\ &= \left(1\text{-}P_{BR}^{(M)}(T)\right)P_{RD}^{(M)}(T) + P_{BR}^{(M)}(T)\left(1\text{-}P_{RD}^{(M)}(T)\right) + P_{BR}^{(M)}(T)P_{RD}^{(M)}(T) \\ &= P_{RD}^{(M)}(T) + P_{BR}^{(M)}(T)\text{-}P_{BR}^{(M)}(T)P_{RD}^{M}(T). \end{aligned} \tag{11}$$

The states of the system successfully receiving the data from the base station include all $S_{m,m}$, that is, $S_{1,1}, S_{2,2}, \cdots, S_{m,m}, \cdots, S_{M,M}$. Then, the total data pass rate of the system is

$$\begin{aligned} P_{pass} &= \sum_{m=1}^{M} S_{m,m} \\ &= \sum_{m=1}^{M} \begin{pmatrix} \left(P_{BR}^{(m\text{-}1)}(T)\text{-}P_{BR}^{(m)}(T)\right)\left(1\text{-}P_{RD}^{(m\text{-}1)}(T)\right) \\ + \left(P_{RD}^{(m\text{-}1)}(T)\text{-}P_{RD}^{(m)}(T)\right)\left(1\text{-}P_{BR}^{(m\text{-}1)}(T)\right) \\ + \left(P_{BR}^{(m\text{-}1)}(T)\text{-}P_{BR}^{(m)}(T)\right)\left(P_{RD}^{(m\text{-}1)}(T)\text{-}P_{RD}^{(m)}(T)\right) \end{pmatrix} \\ &= \left(1\text{-}P_{BR}^{(M)}(T)\text{-}P_{RD}^{(M)}(T) + P_{BR}^{(M)}(T)P_{RD}^{(M)}(T)\right). \end{aligned} \tag{12}$$

The transmission times of state $F_{m,0}$, $F_{0,m}$, $F_{m,m}$, and $S_{m,m}$ are all m times. When the system stops retransmission, the possible states are $F_{M,0}$, $F_{0,M}$, $F_{M,M}$, and all $S_{m,m}$ states. Therefore, the total transmission time of each frame is

$$\begin{aligned} ST &= \text{FT} * \left(M * P(F_{M,0}) + M * P(F_{0,M}) + M * P(F_{M,M}) + \sum_{m=1}^{M}(m * P(S_{m,m}))\right) \\ &= \text{FT} * \begin{pmatrix} M * \left(P_{RD}^{(M)}(T) + P_{BR}^{(M)}(T)\text{-}P_{BR}^{(M)}(T)P_{RD}^{M}(T)\right) \\ + \sum_{m=1}^{M}\left(m * \begin{pmatrix} P_{BR}^{(m\text{-}1)}(T)\text{-}P_{BR}^{(m)}(T) + P_{RD}^{(m\text{-}1)}(T)\text{-}P_{RD}^{(m)}(T) \\ \text{-}P_{RD}^{(m\text{-}1)}(T)P_{BR}^{(m\text{-}1)}(T) + P_{BR}^{(m)}(T)P_{RD}^{(m)}(T) \end{pmatrix}\right) \end{pmatrix}. \end{aligned} \tag{13}$$

When the system is in this state $F_{m,0}(m < M)$, the relay will be in the state of energy collection in the next frame. In addition, the first a part of each frame of the system is also used for energy collection, and the energy collected at this time is $\text{FT} * \eta\sigma_{BR}^2 E_R$. Therefore, the total power of relay energy collection is

$$EH_R = (\alpha)\text{FT} * \eta\sigma_{BR}^2 E_B \sum_{m=1}^{M-1} P(F_{m,0}) + (1-\alpha)\text{FT} * \eta\sigma_{BR}^2 E_B, \tag{14}$$

where η represents the received energy conversion efficiency.

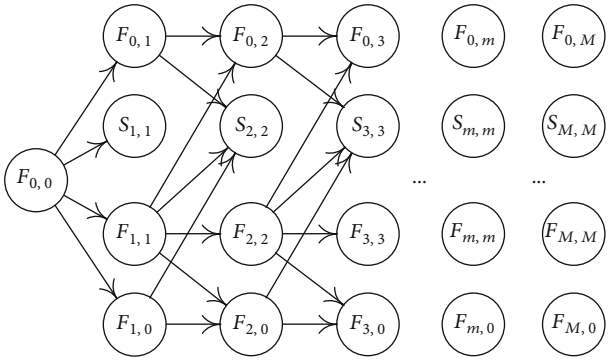

FIGURE 2: The state transition model diagram.

Similarly, the total power of D energy collection in each frame is

$$EH_D = (\alpha)\mathrm{FT} * \eta\sigma_{RD}^2 E_R \sum_{m=1}^{M\text{-}1} P(F_{0,m}) + (1-\alpha)\mathrm{FT} * \eta\sigma_{RD}^2 E_R. \tag{15}$$

In order to better study the relationship between energy transmission and information transmission, the energy transmission power is normalized:

$$\begin{aligned} EH_R^{\mathrm{norm}} &= \frac{EH_R}{EH_R^{\max}} = (1\text{-}\alpha) + \alpha \sum_{m=1}^{M\text{-}1} P(F_{m,0}), \\ EH_D^{\mathrm{norm}} &= \frac{EH_D}{EH_D^{\max}} = (1\text{-}\alpha) + \alpha \sum_{m=1}^{M\text{-}1} P(F_{0,m}), \end{aligned} \tag{16}$$

where $EH_R^{\max} = \mathrm{FT} * \eta\sigma_{BR}^2 E_B$ and $EH_D^{\max} = \mathrm{FT} * \eta\sigma_{RD}^2 E_R$.

Without losing generality, the JNTP (joint normalized throughput of information transmission and energy transmission) is defined as

$$TP = \frac{\left(EH_R^{\mathrm{norm}} + EH_{\mathrm{D}}^{\mathrm{norm}} + \alpha P_{\mathrm{pass}}\right)}{ST}. \tag{17}$$

In the multi-SWIPT relay scenario, relay selection is a very important problem, which can effectively improve the information transmission rate and energy transmission rate of the system [20]. The channel fading of radio wave is related to the transmission distance of information. We assume that the distance between B and R is d_{BR}, the distance between R and D is d_{RD}, and the path loss exponent γ_{L}. According to the large-scale fading multislope model, the relationship between the variance of channel fading and the terminal distance is as follows: $\sigma_{BR}^2 \sim (d_{BR})^{-\gamma_{\mathrm{L}}}$ and $\sigma_{RD}^2 \sim (d_{RD})^{-\gamma_{\mathrm{L}}}$. Therefore, the problem of relay selection can be solved by finding the best relay location (d_{BR}^*, d_{RD}^*):

$$d_{BR}^*, d_{RD}^* = \arg\max TP(d_{BR}, d_{RD}). \tag{18}$$

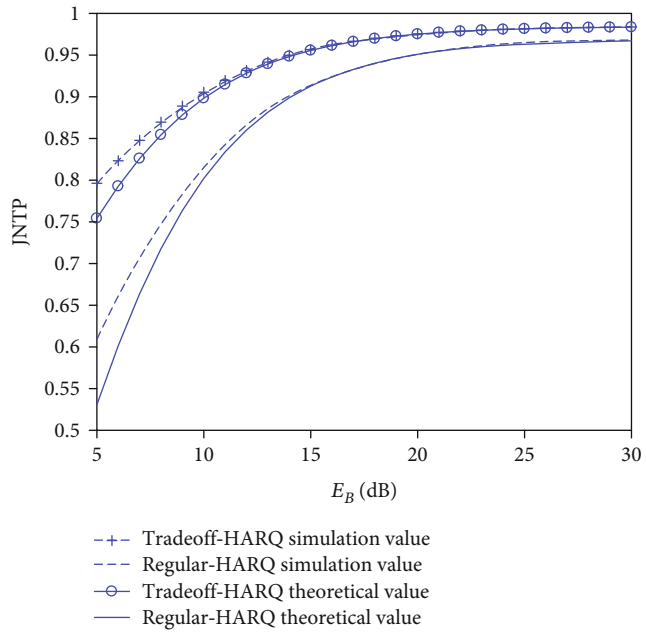

FIGURE 3: The JNTP of the proposed tradeoff-HARQ scheme and the regular-HARQ scheme against E_B.

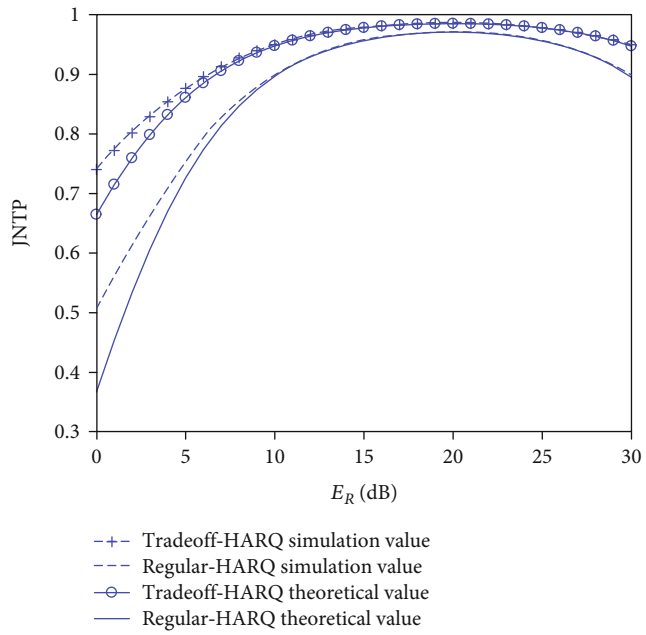

FIGURE 4: The JNTP with E_R under different schemes.

5. Monte Carlo Simulations

In this section, Monte Carlo simulation is used to verify the theoretical value. The simulation software is MATLAB, and the general simulation parameters are as follows: the number of transmission is limited to $M = 3$ (in other words, the number of retransmission is limited to 2), and data rate threshold $T = 1$, $\sigma_{BR}^2 = 1$, $\sigma_{RD}^2 = 1$, and $\sigma_{RR}^2 = 0.01$.

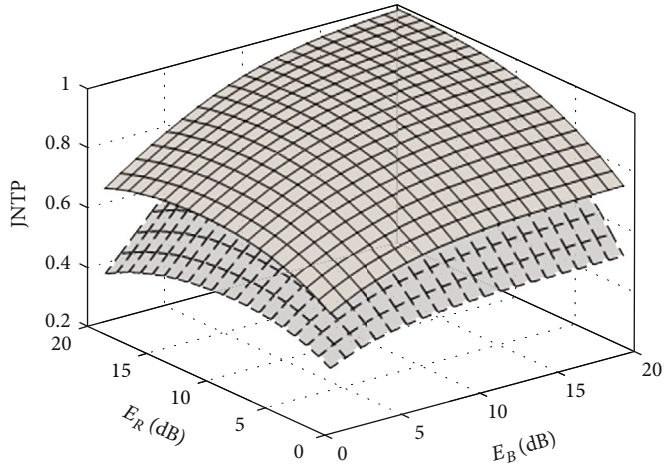

Figure 5: The JNTP curved surface of different schemes.

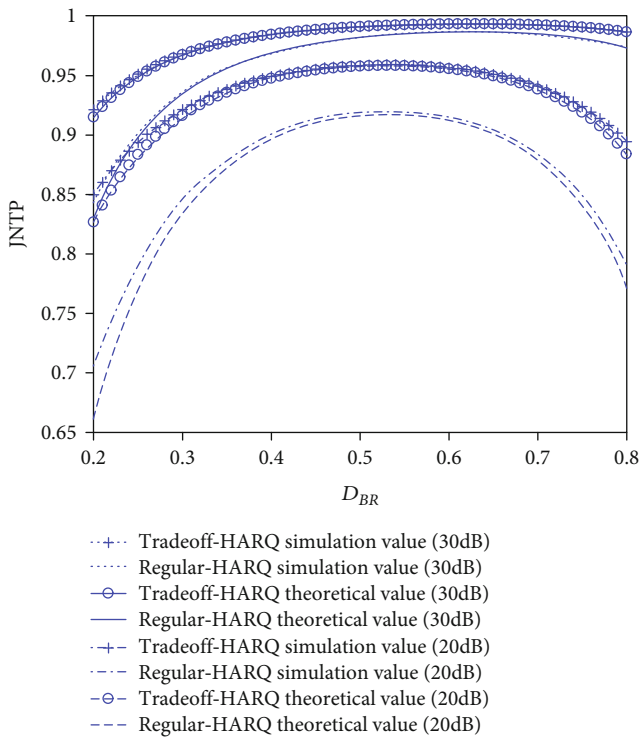

Figure 6: The trend chart of JNTP and distance parameters under different total power limits.

The JNTP of the proposed tradeoff-HARQ scheme and the regular-HARQ scheme against E_B is given in Figure 3. The simulation condition is $E_R = 15$ dB, $\alpha = 0.5$. The "+" and "○" in this figure are the simulation curve and theoretical curve of the JNTP under the tradeoff-HARQ scheme. The unmarked curve is the regular-HARQ scheme. Comparing the theoretical value with the simulation value, it can be seen that there is a small amount of error at low SNR (less than 10 dB), but the error can be ignored at other SNR, so it can be considered that the theoretical value can approximate the simulation value of the JNTP. This figure shows that the JNTP performance of the tradeoff-HARQ scheme is better than that of the regular-HARQ scheme. At low SNR, such as $E_B = 5$ dB, the JNTP of the tradeoff-HARQ scheme is 0.22 higher than that of the regular-HARQ scheme. At high SNR, such as $E_B > 20$ dB, the tradeoff-HARQ scheme is still better than the regular-HARQ scheme, and its advantage is reduced to 0.02.

Figure 4 describes the joint normalized throughput under different schemes with E_R. The simulation condition is $E_B = 15$ dB, $\alpha = 0.5$, and the mark is the same as Figure 3. As shown in this figure, when E_R is close to 20 dB, the JNTP of the proposed tradeoff-HARQ scheme reaches the maximum. The self-interference signal of the relay increase with the relay transmission power, and the received signal to interference noise ratio of the relay decrease with the increase of E_R.

For better insights, the JNTP curved surface of different schemes is illustrated in Figure 5. The dotted line is the regular-HARQ scheme. As shown in this figure, the proposed tradeoff-HARQ scheme is superior to the regular-HARQ scheme in most cases of E_B and E_R. The advantage is obvious in low SNR.

Figure 6 elaborates the change trend of JNTP and distance parameters of different schemes under different total power limits. The simulation condition is that the total power is limited to 20 dB and 30 dB, and the curve mark is shown in this figure. In order to investigate the relationship between relay location and performance, we assume that the distance between B and D is 1, and the distance between B and R is normalized to the distance parameter D_{BR}. For convenience of description, the simulation in Figure 6 assumes that the R is located on the connection between B and D. When the total power is limited to 20 dB and the distance parameter is 0.54, the JNTP of the tradeoff-HARQ scheme and the regular-HARQ reaches the maximum of 0.95937 and 0.92054, and the performance of the tradeoff-HARQ scheme is 0.03883 higher than that of the regular-HARQ. When the total power is limited to 30 dB, the maximum values are 0.99345 and 0.98694, respectively (when the distance parameter is about 0.63). The performance of the tradeoff-HARQ scheme is 0.00651 higher than that of the regular-HARQ scheme.

6. Conclusions

In order to develop the potential of SWIPT DF relay, this paper proposes the tradeoff-HARQ scheme of full-duplex SWIPT DF relay. First of all, the system model and retransmission slot structure are optimized by using the characteristics of full-duplex relay. Then, the state transition model is established by analysing the slot structure. Furthermore, the state probability and transition probability of each state are calculated to obtain the total passing rate, energy collection efficiency, and the total transmission time. Ultimately, in order to compare the performance of various HARQ schemes more effectively, the joint normalized throughput is constructed. Simulation results show that the joint normalized throughput of the proposed tradeoff-HARQ scheme is better than that of the regular-HARQ scheme. When the total power is limited to 20 dB, the performance of the tradeoff-HARQ scheme is 0.03883 higher than that of the regular-HARQ scheme.

Data Availability

The data used to support the findings of this study are included within the article.

Conflicts of Interest

The authors declare that there is no conflict of interest regarding the publication of this paper.

Acknowledgments

This paper was supported by the National Natural Science Foundation of China (61701251, 62071244, 62071249, 61801236, 61806100, and 61872423), the Natural Science Foundation of the Jiangsu Higher Education Institutions of China (20KJB630003), and the Natural Science Foundation of Jiangsu Province (Grant No. BK20160903).

References

[1] I. Krikidis, S. Timotheou, S. Nikolaou, G. Zheng, D. W. Ng, and R. Schober, "Simultaneous wireless information and power transfer in modern communication systems," *IEEE Communications Magazine*, vol. 52, no. 11, pp. 104–110, 2014.

[2] Z. Xie, "Secured green communication scheme for interference alignment based networks," *Journal of Communications and Networks*, vol. 22, no. 1, pp. 23–36, 2020.

[3] A. Abrol and R. K. Jha, "Power optimization in 5G networks: a step towards green communication," *IEEE Access*, vol. 4, pp. 1355–1374, 2016.

[4] Z. Chen, H. Xu, L. X. Cai, and Y. Cheng, "Beamforming design for max-min fair SWIPT in green cloud-RAN with wireless fronthaul," in *IEEE Global Communications Conference (GLOBECOM)*, pp. 1–6, Abu Dhabi, United Arab Emirates, December 2018.

[5] I. Krikidis, "Relay selection in wireless powered cooperative networks with energy storage," *IEEE Journal on Selected Areas in Communications*, vol. 33, no. 12, pp. 2596–2610, 2015.

[6] X. Shi, J. Sun, D. Li, F. Ding, and Z. Zhang, "Rate-energy tradeoff for wireless simultaneous information and power transfer in full-duplex and half-duplex systems," *CMC-Computer Materials and Continua*, vol. 65, no. 2, pp. 1373–1384, 2020.

[7] N. Ashraf, S. A. Sheikh, S. A. Khan, I. Shayea, and M. Jalal, "Simultaneous wireless information and power transfer with cooperative relaying for next-generation wireless networks: a review," *IEEE Access*, vol. 9, pp. 71482–71504, 2021.

[8] G. Pan, "On secrecy performance of MISO SWIPT systems with TAS and imperfect CSI," *IEEE Transactions on Communications*, vol. 64, no. 9, pp. 3831–3843, 2016.

[9] Y. Liu, "Joint resource allocation in SWIPT-based multiantenna decode-and-forward relay networks," *IEEE Transactions on Vehicular Technology*, vol. 66, no. 10, pp. 9192–9200, 2017.

[10] D. Kudathanthirige, R. Shrestha, and G. A. A. Baduge, "Wireless information and power transfer in relay-assisted downlink massive MIMO," *IEEE Transactions on Green Communications and Networking*, vol. 3, no. 3, pp. 789–805, 2019.

[11] C. Tseng and S. Wu, "Selective and opportunistic AF relaying for cooperative ARQ: an MLSD perspective," *IEEE Transactions on Communications*, vol. 67, no. 1, pp. 124–139, 2019.

[12] S. Luo and K. C. Teh, "Amplify-and-forward based two-way relay ARQ system with relay combination," *IEEE Communications Letters*, vol. 19, no. 2, pp. 299–302, 2015.

[13] Z. Shi, C. Zhang, Y. Fu, H. Wang, G. Yang, and S. Ma, "Achievable diversity order of HARQ-aided downlink NOMA systems," *IEEE Transactions on Vehicular Technology*, vol. 69, no. 1, pp. 471–487, 2020.

[14] X. Lu, E. Hossain, H. Jiang, and G. Li, "On coverage probability with type-II HARQ in large-scale uplink cellular networks," *IEEE Wireless Communications Letters*, vol. 9, no. 1, pp. 3–7, 2020.

[15] M. Otaru, M. Ajiya, A. Adinoyi, M. Aljlayl, and H. Yanikomeroglu, "An ARQ-based cooperative relaying scheme for 5G IoT slice," in *IEEE Global Conference on Internet of Things (GCIoT)*, pp. 1–5, Dubai, United Arab Emirates, 2019.

[16] S. Li, F. Wang, J. Gaber, and X. Chang, "Throughput and energy efficiency of cooperative ARQ strategies for VANETs based on hybrid vehicle communication mode," *IEEE Access*, vol. 8, pp. 114287–114304, 2020.

[17] M. S. H. Abad, O. Ercetin, T. ElBatt, and M. Nafie, "SWIPT using hybrid ARQ over time varying channels," *IEEE Transactions on Green Communications and Networking*, vol. 2, no. 4, pp. 1087–1100, 2018.

[18] J. Liu, Q. Rong, and M. Wang, "Adaptive self-interference cancellation in broadband full-duplex MIMO relays," in *Asia-Pacific International Symposium on Electromagnetic Compatibility*, pp. 570–572, Shenzhen, China, May 2016.

[19] R. P. Sirigina and A. S. Madhukumar, "Interference cancellation through interference forwarding in relay-assisted systems," *IEEE Systems Journal*, vol. 12, no. 3, pp. 2373–2384, 2018.

[20] S. Gautam, E. Lagunas, S. K. Sharma, S. Chatzinotas, and B. Ottersten, "Relay selection strategies for SWIPT-enabled cooperative wireless systems," in *IEEE 28th Annual International Symposium on Personal, Indoor, and Mobile Radio Communications*, pp. 1–7, Montreal, QC, Canada, October 2017.